# Simulation and analysis of ion guiding through a nanocapillary in insulating polymers

N. Stolterfoht

*Helmholtz-Zentrum Berlin für Materialien und Energie, D-14109 Berlin, Germany*
(Received 8 August 2012; published 14 January 2013)

The guiding of highly charged ions through a single cylindrical nanocapillary is simulated to compare with previous experiments using capillaries in polyethylene terephthalate (PET) and polycarbonate (PC) polymers. The ions move in the three-dimensional electric field produced by the charges that ions have deposited before. Guiding conditions are achieved, using a nonlinear conductivity law to transport the deposited charges along the capillary surface. Remarkably, it is found that the migration of the deposited charges perpendicular to the capillary axis has a bigger effect on maintaining the ion guiding than the transport parallel to it. The ion trajectories are found to be focused, enhancing the ion guiding. The mean angle of the transmitted ions exhibit pronounced oscillations, in agreement with previous measurements. Experimentally observed differences in the oscillatory frequency as well as partial blocking of the ion transmission are interpreted by the calculations using a larger conductivity for PC in comparison with PET. Emphasis is given to the understanding of the self-organized formation of the charge patches.

## I. INTRODUCTION

During the last decade, the transmission of ions through capillaries with a diameter of a few hundred nm has received considerable attention. Pioneering work has been conducted with metallic capillaries wherein the ions undergo charge transfer processes producing hollow atoms that can leave the capillary exit [1,2]. On the contrary, capillaries in highly insulating materials like polymers collect ions at the wall so that charge patches are created. Sufficient charge collection produces a repulsive electric field, which results in the deflection of the following ions. This deflection occurs at relatively large distances so that electron capture into the projectile is inhibited.

Thus, the ions are guided along the capillary axis maintaining their incident charge state during their passage even when the capillary axis is tilted with respect to the incident beam direction [3]. The capability of insulating capillaries to guide ions at equilibrium is referred to as the guiding power. The fraction $f(\psi)$ of transmitted ions at equilibrium generally decreases exponentially with the square of the tilt angle $\psi$. The guiding power can be quantized by the characteristic *guiding angle* $\psi_c$ for which the normalized transmission fraction drops as $f(\psi_c)/f(0) = 1/e$. To date, the guiding angle is accepted as a convenient parameter to quantify the guiding power.

The initial exploration of the ion-guiding phenomenon in insulating materials have been performed using capillaries in polyethylene terephthalate (PET) polymers (see Refs. [3–5], and references therein). Due to the increasing interest in this field, several laboratories performed experimental studies of capillary guiding with PET [6–11], polycarbonate (PC) [8,12], $SiO_2$ [13], and $Al_2O_3$ [14–17]. Also, electrons were used as projectiles guided through capillaries in $Al_2O_3$ [18] and PET [19]. Moreover, guiding of charged particles have been performed in single-glass capillaries [20–25] and between parallel glass plates [26–28]. Pioneering theoretical studies, based on simulations and *ab initio* calculations, have provided detailed information about the guiding mechanisms [29–33].

The essential property of the ion guiding is the self-organizing process, which governs the charge deposition inside the capillaries [3]. The incident ions produce a predominant charge patch in the entrance region. With increasing deposition of the ions, the charge patch increases until the electrostatic field is large enough to deflect the ions. Then, the charge deposition decreases. However, additional weaker patches are temporarily produced further inside the capillaries, as have been demonstrated in the previous simulations [29,30].

Experimental studies of the temporary charge patches have been conducted more recently [34–37] where oscillatory variations of the ion emission angle have been observed. After sufficient insertion of charges, the ion transmission reaches an equilibrium where the angular oscillations diminish and the number of transmitted ions remains essentially constant. The transmitted ion fraction was found to be nearly constant for an incident ion current changing by two orders of magnitude [5], which provides evidence that the material conductivity is governed by a nonlinear (exponential) conductivity law [4]. To date, agreement exists about the essential properties of the guiding phenomenon; however, many details of the guiding mechanisms are only partially understood.

In this work, simulations of the ion transmission through an insulating capillary are performed, to gain more insight into the self-organized guiding process. Some preliminary results have been presented at recent conferences [38,39]. The present simulations are similar to those performed in the previous series of studies [29–33]. However, essential differences exist between the two theoretical approaches. In this work, the charge transport is modeled by a nonlinear (exponential) dependence of the conductivity from the electric field, whereas the previous studies use a diffusion model wherein the charges perform a random walk. In the limit of small fields the present nonlinear model tends to a linear model, which essentially differs from the diffusion concept. In the following, results of both the linear and nonlinear model are presented. Altogether, particular effort is devoted to the demonstration and analysis of the self-organized charge deposition and ion deflection.

## II. EXPERIMENTAL INFORMATION

In this section a few results from previous experiments are shown to provide motivation for the present simulation and outline the goals of the calculations. The typical nanocapillaries used in the experiments [3,40] have a diameter of $d = 100$ to 200 nm and a length of about $L = 10 \mu$m. Let $J_d$ be the total ion beam current incident on the front surface of the capillary sample. Then, the current $J_{in}$ inserted into a single capillary is obtained as [10]

$$J_{in} = J_d \left( \frac{d}{D} \right)^2, \qquad (1)$$

where $D$ is the diameter of the incident beam. For a typical beam diameter of $D = 1$ mm and a capillary diameter of $d = 200$ nm it follows that $(d/D)^2 = 4 \times 10^{-8}$. Hence, for an ion current of $J_d = 100$ pA the current inserted into the capillary is equal to 0.004 fA.

An important parameter to analyze the ion guiding is the charge $Q_{in}$ inserted into a single capillary. For a constant ion beam the inserted charge is evaluated as $Q_{in} = J_{in}t$, i.e., it is proportional to time $t$. For instance, with the beam of 100 pA the time of 250 s (about 4 min.) is needed to collect a charge of 1 fC. Since the inserted charge is proportional to time one can also speak of the time evolution of measured quantities. Various experimental studies in different laboratories [34–37] have been devoted to the dynamics of the ion guiding.

To study dynamic guiding properties, the intensity of the transmitted ions and the mean angle of the ions ejected from the capillary exit have been measured. Figure 1 shows typical examples for 3 keV Ne$^{7+}$ ions transmitted through nanocapillaries in PET [36,41] and PC [41] polymers plotted as a function of the inserted charge $Q_{in}$. The tilt angle is $\psi = 5°$. In Figs. 1(a) and 1(c) the intensities of the transmitted ions are given and in Figs. 1(b) and 1(d) the corresponding mean angles are depicted. The left-hand column shows results of
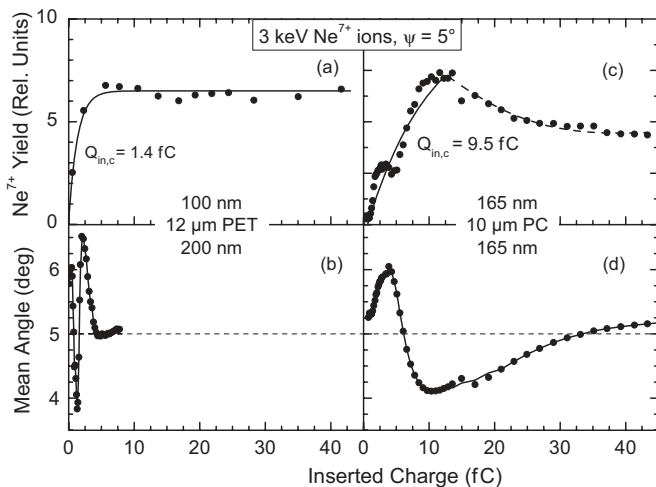


FIG. 1. Comparison of previous results for 3 keV Ne$^{+7}$ ions guided through capillaries in PET [36,41] and PC [41]. The upper panels (a) and (c) show the intensities of the transmitted ions and in the lower panels (b) and (d) the corresponding mean angles are given as a function of the inserted charge $Q_{in}$. Two types of capillaries were used as indicated in the figures and discussed in the text.

PET capillaries with a length of 12 $\mu$m. Figure 1(a) shows data for a capillary diameter of 100 nm and Fig. 1(b) shows data for 200 nm. In the right-hand column results for PC capillaries with a diameter of 165 nm and a length of 10 $\mu$m are given.

The intensity of the transmitted ions generally starts with a certain delay of $Q_{in,s}$, from zero to a maximum value. The initial increase of the ion yield was approximated by the exponential charge-up function [5]

$$Y(Q_{in}) = Y_0 \left( 1 - \exp\left[ -\frac{Q_{in} - Q_{in,s}}{Q_{in,c}} \right] \right), \qquad (2)$$

for $Q_{in} > Q_{in,s}$ and $Y(Q_{in}) = 0$ otherwise. The characteristic charge $Q_{in,c}$ was determined by fitting the total ion yield as shown in Figs. 1(a) and 1(c), where the fit results are given as a solid line in conjunction with the characteristic value of the inserted charge $Q_{in,c} = 1.4$ and 9.5 fC, respectively. For the PET capillaries shown in Fig. 1(a) the intensity remains constant while the intensity for the PC capillaries in Fig. 1(c) decreases after passing a maximum. The latter observation can be interpreted as a partial blocking of the ions.

The blocking of the ion guiding has not been investigated in detail yet. Different effects may contribute to the decreasing ion intensity. A major effect is probably due to the influence of the repulsive field from neighboring capillaries. It should be noted that the density of the PET capillaries is much smaller than that of PC, i.e., $4 \times 10^6$ and $10^8$ cm$^{-2}$, respectively [36,41]. Since the present simulations do not take into account neighbor effects, we shall concentrate on other possibilities for blocking the guided ions. More information about neighbor effects can be obtained from previous simulations which treat a multitude of capillaries [29,30].

The mean angles, presented in Figs. 1(b) and 1(d), exhibit oscillations within $\pm 1.5°$ around the center angle of 5°. These oscillation are qualitatively the same for the two polymers. However, those in Fig. 1(d) for the PC capillaries are significantly stretched with respect to the PET results. This stretching has been a surprise, and is still waiting for an explanation, while the oscillations can be associated with the transient formation of secondary charge patches. Apart from the dominant charge patch near the entrance region, additional weaker patches are temporarily produced further inside the capillaries [30]. The temporary patches play a significant role in the guiding process during the pre-equilibrium period as shown in Fig. 2(a). At equilibrium, represented by Fig. 2(b), the secondary patches lose importance and the transmission stabilizes. However, since the ions are steered primarily along
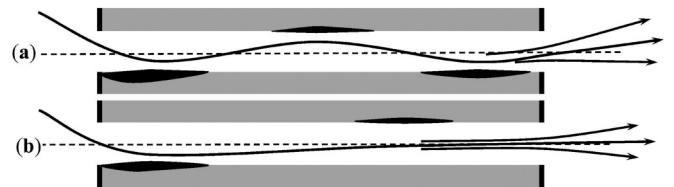


FIG. 2. Scenarios of ion guiding through capillaries in an insulating material. In panels (a) and (b) typical trajectories occurring in, respectively, the dynamic and the equilibrium period of the charge evolution are shown, where the black areas indicate charge patches [41].

the capillary axis, it is expected that smaller charge patches remain within the inner part.

A detailed analysis of the dynamics of the charge patch formation is still missing. The diagrams in Fig. 2 represent an artistic scenario [36] that is not based on theoretical results. The temporary formation of charge patches has been made evident in the previous simulations [29–31], however, those studies have been focused on other aspects of the ion guiding phenomenon. More specific work is needed to interpret the various recent experiments [34–37] concerning oscillations of the ion emission angle and the transient formation of charge patches in the capillary interior.

## III. THEORETICAL METHOD

### A. Basics of calculations

The simulation of the ion guiding is performed in three dimensions using a single capillary of cylindrical symmetry as shown in Fig. 3. Note that the aspect ratio of the cylinder is significantly changed for graphical reasons. The ions are inserted under the tilt angle $\psi$ starting with random $x$ and $y$ values within the circular entrance of the capillary, where $x$ and $y$ are, respectively, the horizontal and vertical coordinates perpendicular to the capillary $z$ axis. A divergence of the incident angle of $\pm 0.3°$ was implemented. Figure 3 exhibits typical trajectories, which are deflected by the electric field produced by deposited charges. Trajectory (1) involves an ion that passes the capillary, while trajectory (2) ends at the wall of the capillary. The incident ions, which impinge on the inner capillary wall, are assumed to deposit their full charge onto the surface. The effect of secondary electrons ejected by the interaction of the ions from the capillary wall is neglected, since it was shown to be small [30].

The electric potential produced by the surface charges was evaluated by accumulating the number of $n$ individual Coulomb potentials of the positive point charges deposited on the capillary surface:

$$V(\mathbf{r}) = \sum_{i=1}^{n} \frac{q_{sc}}{\left(|\mathbf{r} - \mathbf{r}_i|^2 + r_c^2\right)^{1/2}}, \qquad (3)$$
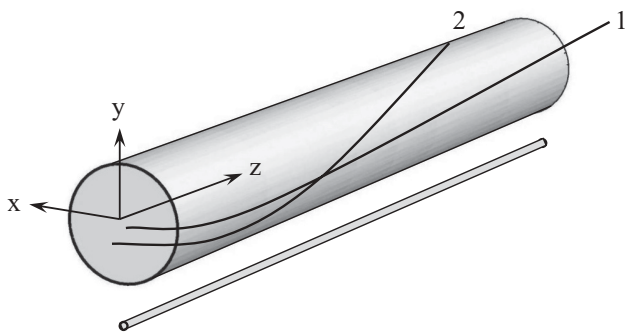


FIG. 3. Cylindrical capillary in three dimensions to visualize ion paths. Trajectory (1) shows the transmission of an ion and trajectory (2) leads to the deposition of an ion at the capillary surface. The aspect ratio is significantly changed for graphical reasons. Also shown is a thin cylinder which demonstrates the real aspect ratio of 50 (ratio of 10 $\mu$m length to 200 nm diameter).

where $\mathbf{r} = (x, y, z)$ is the particle coordinate and $\mathbf{r}_i$ is the position of the $i$th deposited charge whose screened charge is $q_{sc}$. For practical reasons in the calculations, a small distance $r_c$ was introduced to avoid the singularity of the Coulomb potential for $|\mathbf{r} - \mathbf{r}_i| \to 0$. The screened charge is evaluated by means of dielectric screening [32]

$$q_{sc} = q \frac{2}{\varepsilon + 1} \quad \text{or} \quad q_{sc} = q \frac{\varepsilon - 1}{\varepsilon + 1}, \qquad (4)$$

depending on the charge being deposited at the surface or in the bulk, respectively, where $q$ is the deposited projectile charge and $\varepsilon$ is the dielectric constant. For both polymers PET and PC the dielectric constant is $\varepsilon \approx 3$ [42,43], so that the screening reduces the charges deposited at the surface and in the bulk by a factor of two.

In the experiments a conducting Au layer was evaporated on the front and back side of the polymer foils to avoid macroscopic charging outside the capillaries. This grounded metal layer affects the field within the capillary, i.e., in particular, in the region near the entrance and exit of the capillary. The grounded metal layer was taken into account by adding image charges of the deposited ions using the metal layer as a mirror. In an approximation, the metal layer was assumed to be extended covering the entrance and exit holes of the capillary. In this way, negative image charges were virtually placed outside the capillary, which were added when deducing the potential by Eq. (3). The major effect of the negative image charges is that the potentials drop to zero at the entrance and exit of the capillary. This potential was differentiated analytically with respect to the $x$, $y$, and $z$ coordinates yielding the electric field components $E_x$, $E_y$, and $E_z$, respectively.

The ion trajectories within the capillary were evaluated by solving Newton's equations of motion for a particle of positive charge $q$ moving in the electric field $\mathbf{E} = (E_x, E_y, E_z)$:

$$m \frac{d^2 \mathbf{r}}{dt^2} = q \mathbf{E}, \qquad (5)$$

where $\mathbf{r}$ is the coordinate and $m$ is the mass of the ion. We note that the influence of the image charge produced by the capillary surface on the moving ion is neglected. We expect that the image charge plays a role only if the charge deposition is small, e.g., at the beginning of the ion transmission at zero tilt angle, i.e., when the ions are incident parallel to the capillary axis [2].

First, a test calculation is performed under the extreme condition that the charges remain fixed in their position after deposition. Figure 4 shows the results of such a simulation for 3 keV Ne$^{7+}$ ions with a total beam of 100 pA whose diameter is 1 mm. The ions are incident at a tilt angle of $5°$ into a capillary with a width of $d = 200$ nm and a length of $L = 10$ $\mu$m. The values of the parameters are summarized in Table I. Each panel in the left-hand column shows 20 ion trajectories calculated after insertion of the charge $Q_{in}$ indicated in each graph. The distribution of the deposited charges are depicted in the corresponding panels on the right-hand column.

Figure 4(a) shows the formation of a charge patch in the entrance region. The insertion of the total charge of 0.4 fC is not sufficient to significantly affect the ion trajectories. After deposition of 1.2 fC a significant part of the ions are deflected toward the capillary exit. Then, as seen from Fig. 4(b), the
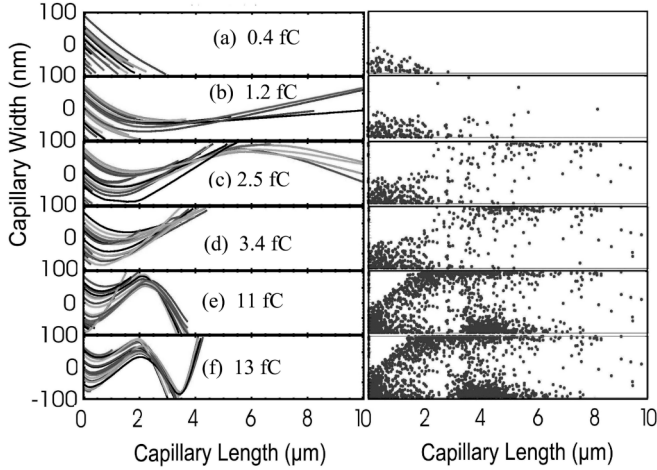
FIG. 4. Trajectories of 3 keV Ne$^{7+}$ (left-hand panels) and corresponding distributions for the deposited charges (right-hand panels). The inserted charge $Q_{in}$ is indicated in each panel. The graphs are projections from cylindrical capillaries treated in three dimensions. The capillaries are transparent so that all deposited charges are visible.

ion guiding starts. With additional charge deposition onto the entrance patch, the ion deflection increases so that the ions hit the opposite wall of the capillary, as seen from Fig. 4(c). There, an additional charge patch is produced which again guides the ions to the capillary exit.

Figures 4(b) and 4(c) indicate focusing effects on the ion beam, i.e., the ion trajectories cross each other within the capillary depth of 4 to 5 $\mu$m. This focusing effect is produced by specific properties of the component $E_y$ of the entrance field, which is stronger at the bottom (at negative $y$ values) than in the center of the capillary. Hence, the trajectories of ions passing near the bottom are more deflected than those passing the capillary center. (Note also the crossing of the two trajectories in Fig. 3.) The focusing is likely to be an important reason for the high fraction of ion transmission associated with the guiding phenomena.

Finally, Figs. 4(d)–4(f) demonstrate that the further enhancement of the entrance patch stops the ion guiding. The entrance patch becomes overcharged and the ions are so strongly deflected that they cannot reach the capillary exit. Consequently, the ion guiding is fully blocked. A similar conclusion has been achieved in the previous simulations [29,30]: when a rather slow removal of the deposited charges was assumed, the charge patches were overcharged so that the

TABLE I. Parameters used for the simulations. The energy and total current of the Ne$^{7+}$ projectile are given together with the diameter, length, and tilt angle of the capillary.

| Parameter | Value |
| --- | --- |
| Energy | 3 keV |
| Current | 100 pA |
| Diameter | 200 nm |
| Length | 10 $\mu$m |
| Tilt angle | 5° |

ions were not able to reach the capillary exit. The agreement of the previous and present simulations is plausible, since without charge transport both calculations are performed with minor approximations. In this extreme case, both simulations represent essentially *ab initio* calculations which involve no adjustable parameter.

However, both simulations indicate that the charge patches have to be reduced to maintain the ion guiding. Therefore, to achieve guiding conditions it is necessary to include the transport of the surface charges. The inclusion of the conductivity is the challenging part of the simulations as will be shown in the next subsection.

### B. Transport of deposited charges

The transport of the deposited charges occurs along the capillary wall via the surface conductivity. In accordance with the material properties of the PET [42] and PC [43] polymers, the surface conductivity $\sigma_s$ plays a dominant role so that it is predominantly focussed on in the following, while the bulk conductivity is treated in an approximation. In accordance with previous experimental studies [4,5], we use here the concept of a nonlinear charge conductivity, which differs from the charge diffusion model previously adopted [30]. Our choice enhances the complexity of the simulations so that the calculations become rather time consuming. Also, it will be shown that the treatment of the charge transport involves essentially one free parameter which has to be adjusted within the analysis.

To obtain information about the surface conductivity $\sigma_s$ produced by the electric field $E = |\mathbf{E}|$, the nonlinear expression by Frenkel [44] is used:

$$\sigma_s = \sigma_0 \exp\left(\sqrt{\frac{E}{E_c}}\right) \quad \text{with} \quad E_c = \frac{\varepsilon(kT)^2}{e^3}, \qquad (6)$$

where $\sigma_0$ is the surface conductivity for $E \to 0$, $k$ the Boltzmann constant, and $T$ is the temperature. The Frenkel formula describes the conductivity produced by thermal electron liberation from deep traps enhanced by the lowering of the potential barrier with a high electric field. The Frenkel formula is based on the electron transition rate into the conduction band, which is given by

$$\Gamma_s = \Gamma_0 \exp\left(\sqrt{\frac{E}{E_c}}\right), \qquad (7)$$

where $\Gamma_0$ is the transition rate for $E \to 0$.

In the simulations we consider the deposition of positively charged ions creating a cluster of holes, which are readily captured at localized centers (traps) at the surface. Unlike a liberated electron, which may freely move within the conduction band, a hole migrates in an insulator by performing a series of individual jumps from one trap to the next one. Each transition requires the liberation of an electron into the conduction band, which fills the trap containing the hole.

Hence, the drift velocity of a hole in the direction of the electric field $\mathbf{E}$ vector is given by

$$\mathbf{v}_s = \frac{\lambda}{\tau}, \qquad (8)$$

TABLE II. Parameters used to evaluate the transport of the charges on the capillary surface for nonlinear and linear field dependence (see text).

| Parameter | Nonlinear | Linear |
|---|---|---|
| $E_c$ (V/nm) | $1.33 \times 10^{-3}$ | $\infty$ |
| $\mu_0$ [nm$^2$/(V s)] | 0.01 | 6 |
| $\Delta t$ (s) | 5.6 | 5.6 |

where $\tau$ is the mean time for a hole hopping between two traps and $\lambda$ is the effective hopping distance along the direction of **E**. The hopping time $\tau$ of the hole is equal to the transfer time of the corresponding electron filling the hole. Since the electron liberation time $1/\Gamma_s$ from a deep trap in an insulator is much longer than its travel time in the conduction band, we neglect the latter one. Then, the hopping time of the hole is obtained as $\tau = 1/\Gamma_s$ and Eq. (8) is converted to $\mathbf{v}_s = \lambda \Gamma_s$. Similarly, one obtains the corresponding expression $\mathbf{v}_0 = \lambda \Gamma_0$ for small $E$ fields. Introducing the hole mobility $\mu_0$ for $E \to 0$ in conjunction with the well-known formula

$$\mathbf{v}_0 = \mu_0 \mathbf{E}, \tag{9}$$

the effective hopping distance can be expressed as $\lambda = \mu_0 \mathbf{E}/\Gamma_0$.

Within a macroscopic time $\Delta t$ one obtains the directed hole transport length as $\Delta \mathbf{s} = \mathbf{v}_s \Delta t$. Finally, combining the different expressions it follows that

$$\Delta \mathbf{s} = \Delta t \mu_0 \mathbf{E} \exp\left(\sqrt{\frac{E}{E_c}}\right). \tag{10}$$

The parameter $E_c$, introduced in Eq. (6), is a characteristic field governing the exponential increase of the surface current. The formula (10) implies two regions where for $E \ll E_c$ the transport length $\Delta \mathbf{s}$ follows a linear field dependence (as in Ohm's law) and for $E \gtrsim E_c$ it is determined by an exponential (nonlinear) dependence. At room temperature the characteristic field is equal to $E_c = 1.33 \times 10^{-3}$ V/nm, as shown in Table II. The present simulations will show that the charge transport takes place primarily within the nonlinear region.

It should be added that the mobility $\mu_0$ is proportional to the surface conductivity $\sigma_0$ introduced in Eq. (6). Hence changing the parameter $\mu_0$ is practically equivalent to changing the conductivity $\sigma_0$. Therefore, in the following the variation of $\mu_0$ will also be referred to as a change of the conductivity $\sigma_0$. For the polymers PET [42] and PC [43] the surface conductivities $\sigma_0$ are roughly equal, i.e., $\sim 10^{-16}$ S and, thus, we expect the same for the mobility $\mu_0$. However, depending on the material and surface preparation the conductivity may vary significantly.

A search in the literature yields results for polymers the mobility that changes by at least eight orders of magnitude [45–47] so that it was difficult to use mobilities from elsewhere. Therefore, we treated the mobility $\mu_0$ as an unknown parameter determined in comparison with the experimental results. It was found that adequate guiding conditions could be achieved with a mobility varying by at least an order of magnitude. Thus, it was first set to an intermediate value of $\mu_0 = 0.01$ nm$^2$/(V s)
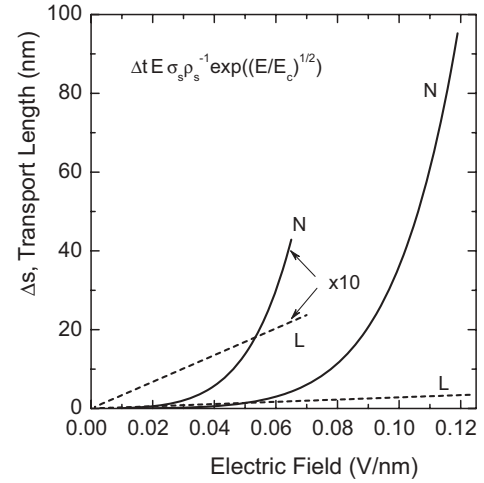


FIG. 5. Transport length of deposited charges in electric field $E$ calculated by means of the parameters in Table II. The curves labeled L and N represent linear and nonlinear versions of Eq. (10) (see text).

(Table II) and varied in a later section. It should be added that the mobilities used here are more than two orders of magnitude smaller than the values found in the literature. This finding will be discussed in some detail below.

To save computing time, the ion insertion and the charge flow were treated sequentially in small portions. After a fixed number $n_0$ of ions (typically $n_0 = 20$ out of several thousands) were inserted into the capillary, the deposited charges were displaced during the time equal to the insertion time $\Delta t$ of $n_0$ ions. This time is given by

$$\Delta t = q n_0 / J_{\text{in}}, \tag{11}$$

where $q$ is again the charge of the incident ion and $J_{\text{in}}$ is obtained from Eq. (1). With the total current of $J_d = 100$ pA one obtains $\Delta t = 5.6$ s. The values of the parameters are summarized in Table II. These values were kept constant throughout the calculations except in the later section, where $\mu_0$ is varied. From Eqs. (10) and (11) it follows that the variation of $\mu_0$ has the same effect as changing the time interval $\Delta t$ or, equivalently, the inverse of the current $J_{\text{in}}$.

Figure 5 depicts the transport length of the deposited charges as a function of the electric field. The curves labeled N are calculated using the nonlinear formula (10) with the corresponding parameter values given in Table II, which were primarily used in the simulations. Nevertheless, for comparison, linear curves labeled L for which $E_c \to \infty$ are shown in Fig. 5. The mobility was arbitrarily set to $\mu_0 = 6$ nm$^2$/(V s) (Table II) to match the two curves at the field of $\sim 0.05$ V/nm, which is a typical value for the simulations. It is noted that the curves labeled N and L differ significantly. The nonlinear curve N exhibits a sharp increase around $E_c = 0.1$ V/nm. The increase is reasonable since around this value the electrical break through along the capillary surface in the PET polymers starts [48].

It is realized that the sequential treatment of the ion insertion and the charge flow involves an approximation. From Eqs. (10) and (11) it follows that the transport length $\Delta \mathbf{s}$ is proportional to the portion $n_0$ of inserted ions. As noted, $n_0 = 20$ was

set leading to the transport length of 1.7 nm for a typical field of 0.05 V/nm in the simulations (Fig. 5). To verify whether this length is reasonably small in comparison with the capillary diameter of 200 nm, a test calculation was performed using a smaller portion of inserted ions. Within statistical uncertainties, the result with $n_0 = 10$ was the same as that for $n_0 = 20$. Hence, we may assume that the sequential treatment of charge insertion and flow involves a reasonable approximation.

The distance and direction of the charge displacement were determined from Eq. (10) with the electric field vector present at the location of the charge under consideration. Thus, the charges were moved along the capillary wall parallel and perpendicular to the capillary $z$ axis. In the latter case, the field projection on the tangent touching the capillary cylinder at the charge location was used. Remarkably, it was found that the charge patches are weakened more by the charge flow along the capillary wall in $x$-$y$ direction than by the flow in the $z$ direction. This is an important conclusion.

Although, the surface conductivity is dominant, the bulk conductivity was included in an approximate manner. Following the methods introduced in previous work [29,30], the bulk conductivity was modeled as a diffusion of the deposited charge entering into the capillary material with probability $p_e$. There, its movement parallel to the surface is neglected assuming a minor bulk mobility. However, the charge is assumed to disappear within the bulk interior with probability $p_b$. This treatment implies a sticking and removal of the deposited charges following exponential decays with time constants $\tau_e = \Delta t / p_e$ and $\tau_b = \Delta t / p_b$, respectively. To restrict the number of variables, $\tau_e = \tau_b$ was assumed for simplicity. In view of previous results [3,30] these parameters were chosen to be equal to 40 minutes. To inquire the sticking effect, simulations were also performed neglecting the sticking and removal of the charges. Hence, different cases for the bulk diffusion are applied as depicted in Table III.

As mentioned before, an ion hitting the capillary wall was assumed to deposit its total charge as a cluster of holes in a single location. Since no surface diffusion was considered, the cluster is transported as a point charge within the local field. However, to avoid irregularities in the calculations produced by the singularity of the Coulomb repulsion between close clusters, the distance of $r_c = 10$ nm was added in the denominator of the Coulomb potential as shown in Eq. (3). This value was chosen because it is about equal to the average distance of adjacent charges in the entrance patch under equilibrium conditions. Moreover, the smoothing of the Coulomb potential may account for the enlargement of the cluster size due to the surface diffusion of the individual holes. In test calculations it was made sure that results of the simulation did not change within the statistical uncertainties,
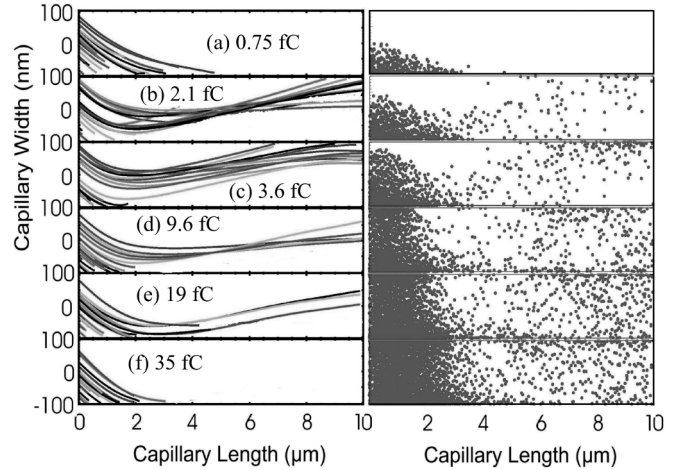


FIG. 6. Trajectories of 3 keV Ne$^{7+}$ (left-hand panels) and corresponding distributions for the deposited charges (right-hand panels). The linear dependence for the charge transport was assumed in accordance with curves L in Fig. 5. The inserted charge $Q_{in}$ is indicated in each panel.

when the 10 nm distance of was increased by factors of two.

The simulations were performed by means of a program written in MATHEMATICA [49]. As noted the present calculations are time consuming primarily due to the use of the nonlinear conductivity law. A full calculation, such as that presented later in figures similar to Fig. 4, requires a computing time of a few days using a fast 3 GHz personal computer.

Before the main calculations are started, a specific simulation is performed using the linear charge transport given by the curves labeled L in Fig. 5. The results of the simulation are presented in Fig. 6 for various values of the inserted charge $Q_{in}$. No bulk diffusion is considered here referring to case (i) in Table III. The trajectories show the usual variation of the mean emission angle. Hence, it can be concluded that the oscillation of the mean emission angle also occurs when a linear charge transport is assumed.

However, Fig. 6(e) indicates that the number of transmitted ions decreases and is totally stopped in Fig. 6(f). The examples show that the ion transmission is totally blocked after a certain charge insertion. This finding is primarily due to the relatively large charge transport for fields $\lesssim 0.05$ V/nm (Fig. 5). The surface migration of the charges perpendicular to the capillary axis to the other side of the entrance charge patch is so strong that the deflection field for the ions diminishes. Hence, the ion guiding cannot be maintained when the charge transport is too high, as similarly noted in previous simulations [29,30].

The foregoing results in Figs. 4 and 6 indicate that ion guiding is not possible outside a certain range of surface conductivity. The size of this range will be studied in more detail in a later section. Here, it shall only be noted that ion guiding can also be maintained with the linear field dependence of the charge transport. For instance, guiding is possible, when the mobility used for the linear model (Fig. 5) is reduced by a factor of two. However, the experience with the present calculations show that the conductivity range, wherein guiding

TABLE III. Decay parameters used for bulk diffusion (see text).

| Case | $\tau_e$ | $\tau_b$ |
|---|---|---|
| (i) no sticking, no removal | $\infty$ | $\infty$ |
| (ii) no sticking, with removal | $\infty$ | 40 min |
| (iii) with sticking, with removal | 40 min | 40 min |

can be achieved, is much smaller for the linear transport model than for the nonlinear model.

## IV. RESULTS OF SIMULATIONS

### A. Trajectories and mean emission angle

In the following, the calculations are devoted to the nonlinear charge transport in accordance with the curves labeled N in Fig. 5. The simulations are performed with the surface conductivity and the usual parameters given in Tables I and II. The bulk conductivity was treated with charge sticking and removal as for case (iii) in Table III. In Fig. 7 trajectories and deposited charges are shown for different inserted charges $Q_{in}$. Figures 7(d)–7(f) indicate that the ions are not blocked. They follow oscillatory trajectories to the end of the capillary where they leave under varying angles. Finally, the ions are emitted parallel to the capillary axis in agreement with the experiments (Fig. 1). Altogether, the simulated results are in general agreement with the predicted scenario shown in Fig. 2.

In the right-hand column of Fig. 7 the distributions of deposited charges are shown. In Fig. 7(a) the trajectories are all stopped at the capillary surface. However, the deposited charge of $Q_{in} = 0.67$ fC produces a field component $E_y$ that weakly deflects the ions so that they land at a location further inside the capillary. Thus, the length of the entrance charge patch is more than doubled. This doubling is part of the self-organizing process of the ion guiding. If the entrance patch becomes saturated in height due to the strong nonlinear charge removal, the patch is extended in length until it is able to deflect the ions towards the capillary exit [41].

In Fig. 7(b) the deflection of the ions to the capillary exit can be seen. Also, the focusing of the ion trajectories is observed as before in Fig. 4(b). As mentioned, this focusing is due to the increase of the field component $E_y$ as $y$ approaches the bottom of the capillary. However, from Figs. 7(c)–7(f) it is seen that the ion focusing diminishes as the charge deposition
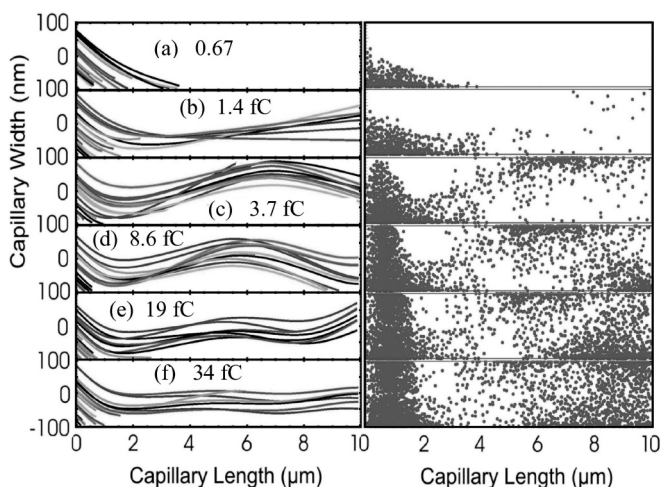
on the entrance charge patch increases. This can be explained by the migration of the charges to the side opposite the entrance charge patch so that the field component $E_y$ becomes constant in the $y$ direction.

In the Figs. 7(c)–7(e) one can clearly distinguish the extended entrance patch from two additional charge patches near the center and the exit of the capillary. The additional patches are transient by changing their position and strength. Finally, in Fig. 7(f) the ion guiding approaches equilibrium, in which the charges are distributed all over the capillary wall as a result of an extensive charge transport. In particular, the entrance charge patch reveals the migration of the charges along the wall perpendicular to the capillary axis. A significant amount of charges are visible in the upper half of the capillary, which cannot directly be reached by the incident ions. This migration to the opposite side of the capillary wall is an important effect that weakens the field produced by the charge patch.

To obtain quantitative information about the ions emerging from the capillary exit, the transmitted ion fraction $f_t = n_t/n_0$ and the mean angle $\overline{\alpha} = n_t^{-1} \sum_i^{n_t} \alpha_i$ was evaluated, where $\alpha_i$ is the emission angle of the $i$th ion and $n_t$ is the total number of transmitted ions (again, $n_0$ is the total number of inserted ions). Figure 8 shows the results for both quantities $f_t$ and $\overline{\alpha}$. To test the influence of the charge sticking and removal, different scenarios are considered. Figures 8(a) and 8(d) show results without charge sticking and removal referred to as case (i) in Table III, Figs. 8(b) and 8(e) show calculations without sticking but with removal referred to as case (ii), and Figs. 8(c) and 8(f) exhibit results with charge sticking and removal referred to as case (iii).

From Figs. 8(a)–8(c) it is seen that the transmitted ion fractions $f_t$ are similar for all cases. The fraction $f_t$ is equal to



FIG. 7. Trajectories of 3 keV Ne$^{7+}$ (left-hand panels) and corresponding distributions for the deposited charges (right-hand panels). The data are based on the nonlinear charge transport in accordance with the curves N in Fig. 5. The bulk conductivity was treated as in case (iii) indicated by Table III for charge sticking an removal. The inserted charge $Q_{in}$ is indicated in each panel.
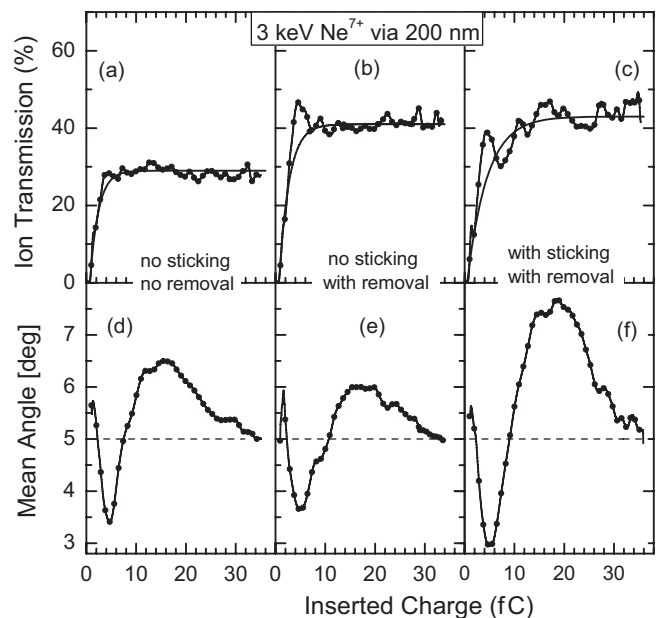


FIG. 8. Transmitted ion fraction $f_t$ and mean emission angle $\overline{\alpha}$ obtained from the analysis of the trajectories shown, e.g., in Fig. 7. The solid lines in the upper panels represent fits to the data using Eq. (2). Different cases are assumed for the charge sticking and removal as defined in Table III and described in the text.

zero for a short interval in accordance with the trajectories in Fig. 7(a). Then, from a certain threshold it rises to an equilibrium value of 30% to 40%, where it remains constant. The constancy of the ion transmission is in accordance with the experimental data for PET [Fig. 1(a)]. To allow for a comparison of the absolute value of 30% to 40% with experiments, additional calculations were performed using 3 keV ions directed into an untilted capillary. In this case, a transmitted ion fraction of 88% was obtained, which is plausible in view of the beam divergence of $\pm 0.3°$. Also, preliminary results for tilt angles of $3°$ and $7°$ were calculated. The calculations result in a guiding angle of $5.6°$, for which the intensity drops to $1/e$ assuming an exponential dependence with the squared tilt angle. The guiding angle is in excellent agreement with the experimental value of $5.3°$ used to set up corresponding scaling rule [8].

In Figs. 8(d)–8(f) the mean angle of the ions exhibits oscillations around the center angle of $5°$ (equal to the tilt angle). The oscillations can be verified from the trajectories in the left-hand column of Fig. 7. First, the ions are deflected from the entrance patch directly to the exit where they leave under angles $\lesssim 6°$, i.e., the sum of the center angle of $5°$ and the aspect angle of $1°$ [Fig. 7(b)]. Then the mean angle oscillates from values smaller than the center angle due to the deflection at the first transient charge patch [Fig. 7(c)] and to values larger than the center angle due to the second transient charge patch [Fig. 7(e)]. These oscillations are in qualitative agreement with the experimental results.

Also, the oscillations of the mean emission angle are similar for the different cases of charge sticking and removal. It is seen from Fig. 8(e) that the charge removal alone decreases the amplitude of the oscillations, whereas Fig. 8(f) indicates that the charge sticking increases the amplitude beyond the values observed in the experiments (Fig. 1). The charge sticking has a similar effects as reducing the surface conductivity. In fact, it is plausible that a strong enhancement of the sticking probability would lead to ion blocking similarly as that demonstrated in Fig. 4.

### B. Potential and field components

To gain more information about the ion guiding mechanism, specific electrical quantities are analyzed in the following. Within the capillary, we consider the potential and field components following from results presented in Figs. 8(b) and 8(e), which refers to the case (ii) for the bulk diffusion (Table III). The intermediate case (ii) corresponds to equal mobilities in the surface and bulk which is a reasonable assumption for polymers. In Fig. 9 the results for $x = 0$ and three different $y$ values are plotted along the $z$ axis. The solid line with points, the solid line, and the dashed line represent data for $y = -65$, 0, and 65 nm, respectively. The inserted charge is equal to 9.5 fC, which is a typical value within the dynamic period of the guiding process. In this period, two transient charge patches are produced apart from the dominant entrance patch (see Fig. 7).

In Fig. 9(a) the potentials exhibit a maximum near the entrance charge patch. Moreover, the potentials are enhanced at the locations of the additional two charge patches. As mentioned, the potential drops to zero at the entrance and
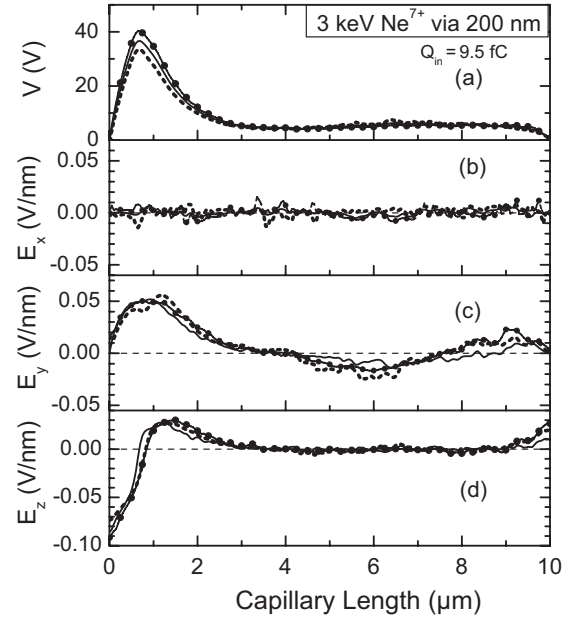


FIG. 9. Potential $V$ and field components $E_x$, $E_y$, and $E_z$. The data are calculated with the parameters given in Table I and a charge insertion of $Q_{in} = 9.5$ fC. The solid line with points, the solid line, and dashed lines represent data for $y = -65$, 0, and 65 nm, respectively, where $x = 0$. The field $E_x$ refers to $x = -65$, 0, and 65 nm with $y = 0$.

exit opening where grounded metal layers are located. Starting from the capillary entrance, the potential rises rapidly producing a field component $E_z$ that reaches the value of 0.1 V/nm [see Fig. 9(d)]. In view of Fig. 5, this field is close to the breakthrough value for polymers so that the charges near the capillary entrance are transported with high probability to the grounded metal layer. Similarly, an opposite $E_z$ field component is produced that transports charge away from the patch center further inside the capillary. Altogether, the entrance charge patch is weakened by this longitudinal transport along the capillary $z$ axis.

As shown in Fig. 9(b), the field component $E_x$ is rather small. It consists essentially of statistical noise produced by ion charges randomly deposited at the capillary wall. In principle, when solving the differential equation (5), the field component $E_x$ may be neglected to save computing time. Nevertheless, $E_x$ was included in the calculations since it was not known *a priori* whether it is always negligible. However, $E_x$ turned out to be small in all calculations so that it will not be discussed any more in the following.

Next, we look back at the three potential curves associated with the different $y$ values. The variation of the potential with respect to the $y$ axis is responsible for the field component $E_y$ depicted in Fig. 9(c). The field component $E_y$ has a maximum near the entrance charge patch reaching 0.05 V/nm. Moreover, significant $E_y$ fields are present at the additional charge patches. At the entrance patch, $E_y$ remains nearly constant when $y$ changes. Therefore, the ions entering at different $y$ values follow parallel trajectories [see Figs. 7(c)–7(f)], i.e., in this case the ion focusing is small. However, small focusing effects are present at the additional charge patches where $E_y$ changes monotonically along the $y$ axis. Hence, the focusing
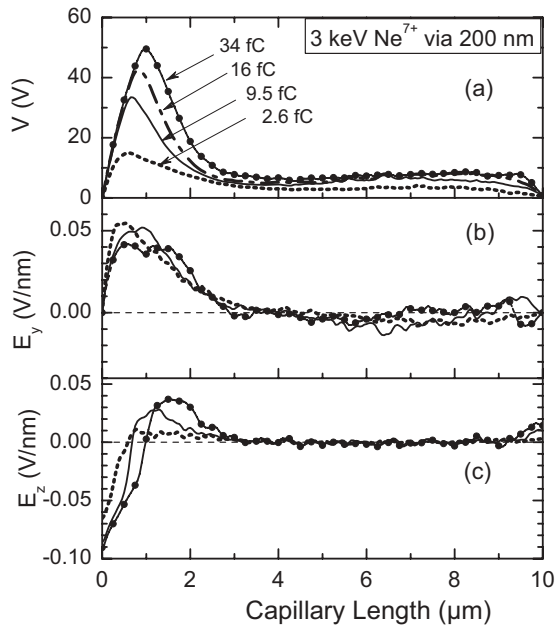
FIG. 10. Potential $V$ and field components $E_y$ and $E_z$. The data are calculated with the parameters shown in Table I. The dotted line, solid line, and solid line with points represent data for $Q_{in} = 2.6$, 9.5, and 34 fC, respectively, where $x = y = 0$. Panel (a) shows an additional dash-dotted line that corresponds to 16 fC.

can be considered as a general phenomenon that supports the ion guiding.

Figure 10 shows potential and field components for additional values of the inserted charge $Q_{in}$. It ranges over the dynamic period of the guiding process until equilibrium is reached at the highest value of $Q_{in}$. As seen in Fig. 10(a), with increasing $Q_{in}$ the maximum of the potential is shifted inside the capillary. The same shift is expected for the entrance patch due to the longitudinal transport of the deposited charges to the metal layer. The corresponding shift can also be seen for the field component $E_z$ depicted in Fig. 10(c).

After reaching equilibrium, the maximum of the potential $V$ is found to be as high as 50 V. This value is still an order of magnitude smaller than 420 V needed to create an potential barrier that cannot be overcome by the 3 keV Ne$^{7+}$ ions. One might suppose that a further increase of the inserted charge will finally create a barrier that is large enough to inhibit the ions passing the capillary. However, it should be realized that the potential maximum is not proportional to the inserted charge as can be seen from the curves in Fig. 10(a). This finding is a result of the loss of the transported charges enhanced by nonlinearity of the conductivity function (Fig. 5). Hence, it is likely that the potential maximum saturates at a value smaller than 420 V. In this case, no blocking of the ions by a potential barrier would occur in a single capillary.

The major effect of the field component $E_y$ is the deflection of the incident ions towards the capillary exit and the migration of the deposited charges perpendicular to the capillary axis. Surprisingly, the trajectories in Fig. 7 show that the ion deflection decreases with increasing charge insertion. This counter intuitive observation is in accordance with the field component $E_y$ shown in Fig. 10(b). The solid line with points, which is

associated with the highest $Q_{in}$ value, exhibits the smallest maximum near the entrance patch. It should be emphasized that this observation enlightens the self-organizing mechanism that maintains the guiding process and produces the oscillations of the mean emission angle. In particular, the equilibrium involves a well-tailored charge patch that ensures a direct ion transmission from the capillary entrance to the exit without being much affected by the other charge patches [see Fig. 7(f)].

The decrease of the field component $E_y$ with the inserted charge is not evident. The charge removal from the entrance patch increases with increasing $Q_{in}$ which is supposed to reduce that patch. On the other hand, when the component $E_y$ decreases, less ions are deflected so that the charge deposition increases. Obviously, the deposition of new charges is less efficient than the charge removal. This stronger charge release is the key for the self-organization of the patch that leads to a steady ion transmission at equilibrium. A plausible explanation for the stronger charge release is that it occurs in two directions, i.e., via the $z$ and $y$ axes, while the charge deposition is governed only by one direction along the $y$ axis.

Finally, at equilibrium, the charge release from the entrance patch must become weaker since, otherwise, the field $E_y$ would be too small to deflect the ions toward the capillary exit. Thus, the guiding cannot be maintained, resulting in a total blocking of the ion transmission. Such a blocking due to an decreasing deflection field $E_y$ was demonstrated by Fig. 6 being in contrast with Fig. 7 where the guiding continues. The next section presents further examples for which the charge release is well balanced at equilibrium.

### C. Variation of conductivity

As mentioned, heretofore the simulations were performed using a set of fixed parameters. All parameters are based on physical grounds except for the surface conductivity and the bulk diffusion. In this subsection, the surface hole mobility $\mu_0$ is varied over an order of magnitude. Moreover, for the bulk diffusion, the cases (ii) and (iii) from Table III are considered. In particular, the attempt is made to interpret the differences between the experimental results for PET and PC (Fig. 1).

Figure 11 shows results for the transmitted ion fraction $f_c$ and the mean emission angle $\overline{\alpha}$. Again, the same parameters are used as before (Table I). The left-hand column in Fig. 11 is associated with the lower mobility [$\mu_0 = 0.003$ nm$^2$/(V s)] whereas the right-hand column is due to a factor of $\sim$10 higher mobility [$\mu_0 = 0.04$ nm$^2$/(V s)]. The mobilities used in this figure are summarized in Table IV. It is recalled that the results presented above in Fig. 8 were obtained with a value of $\mu_0 = 0.01$ nm$^2$/(V s) that lies in between those used here.

TABLE IV. Mobility values $\mu_0$ used in simulations shown in Fig. 11. Also given are the bulk diffusion parameters $\tau_e$ and $\tau_b$ as indicated in Table III.

| Figure | $\mu_0$ | $\tau_e$ and $\tau_b$ |
|---|---|---|
| 11(a) and 11(c) | 0.003 nm$^2$/(V s) | Case (iii) |
| 11(e) | 0.003 nm$^2$/(V s) | Case (ii) |
| 11(b) and 11(d) | 0.04 nm$^2$/(V s) | Case (iii) |
| 11(f) | 0.04 nm$^2$/(V s) | Case (ii) |
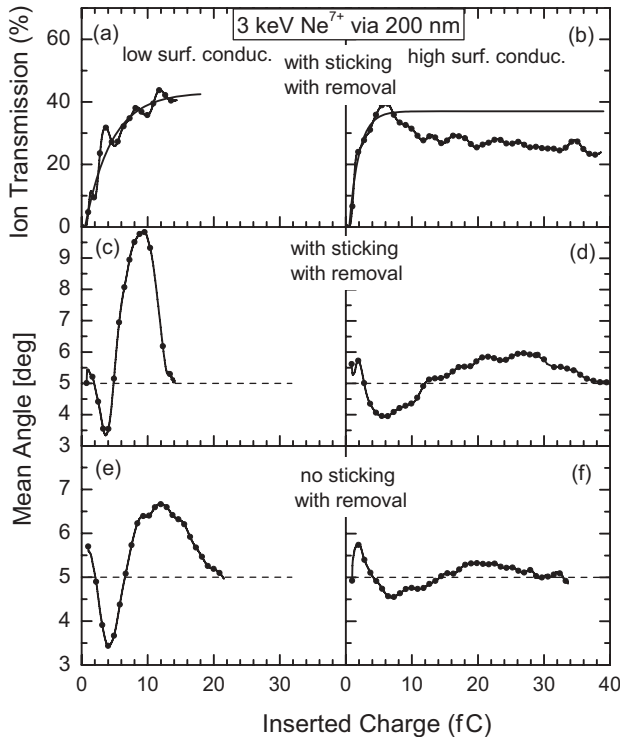
FIG. 11. Fraction of ion transmission $f_t$ and mean angle $\overline{\alpha}$ of 3 keV Ne$^{7+}$ ions ejected from capillary exit. The data in the left- and right-hand columns are obtained with, respectively, a higher and lower surface conductivity associated with the mobility parameters given in Table IV. Different cases for the bulk diffusion are considered (see text).

Essential differences are observed between the results obtained with the two $\mu_0$ values. Let us first compare the data in Figs. 11(a) and 11(b) including charge sticking and removal. For both mobilities the transmitted ion fraction rises with a certain delay from zero to a maximum value. As before, the data were fit by Eq. (2) shown by solid lines. After the maximum is reached the transmitted ion fraction in Fig. 11(a) remains constant with increasing charge insertion, while the ion fraction slightly decreases in Fig. 11(b). This decrease may be considered as a partial blocking of the ions.

Figures 11(c) and 11(d) compare the mean emission angle of the transmitted ions for the two $\mu_0$ values. It is found that the lower mobility produces an oscillation that is higher in frequency and amplitude (left-hand panel) than the one following from the higher mobility (right-hand panel). The reason for the smaller frequency is the faster charge transport, i.e., more charge is needed to create the additional charge patches, which are needed for the oscillations in the ion transmission.

Figures 11(e) and 11(f) depict results for calculations without sticking but with removal (see also Table IV). As shown before in Fig. 8(e) the charge removal has the effect of decreasing (damping) the oscillation amplitude, which is more consistent with the experiments. The comparison of the experimental results in Fig. 1 with the present calculations in Fig. 11 suggests that the differences experimentally observed are due to a higher surface conductivity of PC in comparison to PET. One can see that the constancy of the transmitted ion fraction and the faster oscillation of the mean emission angle agrees with the

experimental PET results, whereas both the partial blocking and the slower oscillation of the mean angle can be observed in the experimental PC results. In particular, it is noted that the mean emission angle $\overline{\alpha}$ for PC in Fig. 1(d) shows a good agreement of with the theoretical results obtained without bulk diffusion [39]. This agreement suggests that the bulk diffusion plays a less important role for the capillaries in PC.

It should be realized, however, that a direct comparison of the theoretical and experimental results is difficult, since different capillary diameters were used. The simulations were performed with a capillary diameter of 200 nm, whereas the experiments with PET and PC refer to 100 (200) and 165 nm, respectively. Also, the experiments involve contributions of millions of capillaries while the theory refers to a single capillary only. Hence, one should not expect a full agreement between theory and experiment. This is particularly true for the experiments with the PC polymer, for which neighbor effect may be important due to the relatively high capillary density.

Finally, we focus the attention on the absolute value of the transmitted ion fraction $f_t$. Remarkably, the maximum value of $f_t$ is nearly constant close to 30% to 40% (Figs. 8 and 11), although the conductivity changes by more than a factor of 10. These intensities correspond to characteristic guiding angles barely changing within $5.2°$ to $5.6°$. This counter intuitive observation can be explained by the fact that the maximum of the ion fraction is reached rather early, i.e., at the beginning of the patch formation where the charge release is still of minor importance. Later, the nonlinearity of the charge transport supports the constancy of the ion transmission. Thus, it follows for a given tilt angle that the maximum of the ion transmission is rather independent of the conductivity.

As noted in conjunction with Eqs. (10) and (11), instead of varying the conductivity, the same results can be achieved by changing the inverse of the ion current $J_{in}$. Therefore, the results in Fig. 11 can also be obtained by keeping the mobility at $\mu_0 = 0.01$ nm$^2$/(V s) and changing the total current from 330 pA (left-hand column) to 25 pA (right-hand column). Thus, it may be concluded that the maximum of the ion transmission changes only marginally with varying ion current. This conclusion is in agreement with the results of ion guiding experiments where the ion beam was changed by about two orders of magnitude [36].

## V. CONCLUSIONS

The simulations of the ion trajectories allowed for several interpretations of the ion guiding mechanisms. First of all, the transport of the deposited ions has to be implemented to avoid the overcharging of the charge patches, which would lead to a blocking of the ion transmission. On the other hand, an enhanced charge release can lead to a decreasing field strength in the entrance region which inhibits a sufficient ion deflection. Between these extremes, the ion guiding is perpetuated within a relative large range wherein the conductivity varies by at least an order of magnitude. Equivalently, the ion beam intensity can be varied by an order of magnitude without changing much the fraction of transmitted ions. This is primarily due to the application of a nonlinear charge transport derived from Frenkel's theory [44].

The hole mobility used in the simulations was determined in comparison with the experimental data. It is noted that this mobility is two to three orders of magnitude smaller than the data found in the literature [45–47]. The mobility of charge carriers is influenced by impurities in the polymer. Since the mobility is based on a hopping mechanism, it is strongly dependent on the depth of the traps involved. In most cases the results for the mobility is determined by experimental methods where free charge carriers (electrons) are excited by external particle impact (photons [46] or electrons [47]). In the present case, where holes are produced by deposition of positive charge clusters on a surface, future work is needed to obtain more information about the charge carrier mobility.

The large differences between PET and PC in the amount of charge insertions were investigated. The capillaries in the PET polymer exhibit a constant transmission with increasing charge insertion whereas the PC polymer indicates partial blocking effects on the transmitted ions. In agreement with experiments, the model calculations indicate that more charge is needed for the PC polymer which obviously has a higher conductivity. Also, it appears that for PC the bulk diffusion is of less importance. The bulk diffusion was introduced in previous simulations [29,30] to account for the relatively long decay time of the ion transmission measured after stopping the incident ion beam [3]. It should be noted, however, that the bulk diffusion is not a stringent condition for ion guiding as the long decay time can also be modeled by the nonlinear surface conductivity [4].

Novel conclusions were drawn from the calculations. The charge transport occurs in two dimensions, i.e., parallel and perpendicular to the capillary axis. It is found that the parallel transport leading to the capillary entrance and exit does not play a dominant role. Remarkably, the major part of the charge patch reduction takes place via the perpendicular charge transport occupying the other side of the capillary wall.

Therefore, the equilibrium condition for the ion transmission is already reached when the charge deposition is still significant. In fact, the simulations show that a large amount of charge may be inserted inside the capillary without forming a potential barrier against the ions. Hence, the period in which the incoming and outgoing charge fluxes are balanced is expected to occur much later than the instant at which the equilibrium of the ion transmission is reached.

The decisive mechanism governing the ion guiding concerns the self-organized formation of the entrance patch. At the beginning of the charge patch creation the entrance field weakly deflects the ions so that they land further inside the capillary. This extension of the charge deposition increases the width and efficiency of the entrance patch so that it becomes capable of deflecting the ions to the capillary exit. After further charge deposition the ions are more deflected, hitting the opposite capillary wall where they form a secondary charge patch which, in turn, creates a third one further inside. Then, as shown in the simulations, after a certain delay, the charge release from the entrance patch becomes more effective so that the ion deflection decreases until the ions are moved directly to the capillary exit. This time delay (retardation) of the charge release is the key for the oscillatory behavior of the ion emission and it governs the ion guiding at equilibrium. It is sensitively dependent on the time required for the migration of the charge to the other side of the capillary. The retardation of the charge release is a remarkable phenomenon of the ion guiding mechanism, and merits further investigations.

### ACKNOWLEDGMENTS

[1] S. Ninomiya, Y. Yamazaki, F. Koike, H. Masuda, T. Azuma, K. Komaki, K. Kuroki, and M. Sekiguchi, Phys. Rev. Lett. **78**, 4557 (1997).

[2] K. Tökési, L. Wirtz, C. Lemell, and J. Burgdörfer, Phys. Rev. A **61**, 020901 (2000).

[3] N. Stolterfoht, J. H. Bremer, V. Hoffmann, R. Hellhammer, D. Fink, A. Petrov, and B. Sulik, Phys. Rev. Lett. **88**, 133201 (2002).

[4] N. Stolterfoht, R. Hellhammer, Z. D. Pešić, V. Hoffmann, J. Bundesmann, A. Petrov, D. Fink, and B. Sulik, Vacuum **73**, 31 (2004).

[5] N. Stolterfoht, R. Hellhammer, J. Bundesmann, D. Fink, Y. Kanai, M. Hoshino, T. Kambara, T. Ikeda, and Y. Yamazaki, Phys. Rev. A **76**, 022712 (2007).

[6] G. Víkor, R. R. Kumar, Z. Pešić, N. Stolterfoht, and R. Schuch, Nucl. Instrum. Methods Phys. Res., Sect. B **233**, 218 (2005).

[7] Y. Kanai, M. Hoshino, T. Kambara, T. Ikeda, R. Hellhammer, N. Stolterfoht, and Y. Yamazaki, Nucl. Instrum. Methods Phys. Res., Sect. B **258**, 155 (2007).

[8] N. Stolterfoht, R. Hellhammer, Z. Juhász, B. Sulik, V. Bayer, C. Trautmann, E. Bodewits, A. J. de Nijs, H. M. Dang, and R. Hoekstra, Phys. Rev. A **79**, 042902 (2009).

[9] M. Kreller, G. Zschornak, and U. Kentsch, J. Phys: Conf. Ser. **163**, 012090 (2009).

[10] N. Stolterfoht, R. Hellhammer, Z. Juhász, B. Sulik, E. Bodewits, H. M. Dang, and R. Hoekstra, Phys. Rev. A **82**, 052902 (2010).

[11] Z. Juhász, B. Sulik, R. Rácz, S. Biri, R. J. Bereczky, K. Tökési, Á. Köver, J. Pálinkás, and N. Stolterfoht, Phys. Rev. A **82**, 062903 (2010).

[12] D. Li, Y. Wang, Y. Zhao, G. Xiao, D. Zhao, Z. Xu, and F. Li, Nucl. Instrum. Methods Phys. Res., Sect. B **267**, 469 (2009).

[13] M. B. Sahana, P. Skog, G. Víkor, R. T. RajendraKumar, and R. Schuch, Phys. Rev. A **73**, 040901 (2006).

[14] S. Mátéfi-Tempfli, M. Mátéfi-Tempfli, L. Piraux, Z. Juhász, S. Biri, É. Fekete, I. Iván, F. Gáll, B. Sulik, G. Víkor *et al.*, Nanotechnology **17**, 3915 (2006).

[15] P. Skog, I. L. Soroka, A. Johansson, and R. Schuch, Nucl. Instrum. Methods Phys. Res., Sect. B **258**, 145 (2007).

[16] Y.-F. Chen, X.-M. Chen, F.-J. Lou, J.-Z. Zhang, J.-X. Shao, G.-Z. Sun, J. Wang, F.-Y. Xi, Y.-Z. Yin, X.-A. Wang *et al.*, Chin. Phys. B **18**, 2739 (2009).

[17] Z. Juhász, B. Sulik, S. Biri, I. Iván, K. Tökési, É. Fekete, S. Mátéfi-Tempfli, M. Mátéfi-Tempfli, G. Víkor, E. Takács *et al.*, Nucl. Instrum. Methods Phys. Res., Sect. B **267**, 321 (2009).

[18] A. R. Milosavljević, G. Víkor, Z. D. Pešić, P. Kolarž, D. Šević, B. P. Marinković, S. Mátéfi-Tempfli, M. Mátéfi-Tempfli, and L. Piraux, Phys. Rev. A **75**, 030901(R) (2007).

[19] S. Das, B. S. Dassanayake, M. Winkworth, J. L. Baran, N. Stolterfoht, and J. A. Tanis, Phys. Rev. A **76**, 042716 (2007).

[20] T. Ikeda, T. M. Kojima, Y. Iwai, Y. Kanai, T. Kambara, T. Nebiki, T. Narusawa, and Y. Yamazaki, J. Phys.: Conf. Ser. **58**, 68 (2007).

[21] A. Cassimi, L. Maunoury, T. Muranaka, B. A. Huber, K. R. Dey, H. Lebius, D. Lelièvre, J. M. Ramillon, T. Been, T. Ikeda *et al.*, Nucl. Instrum. Methods Phys. Res., Sect. B **267**, 674 (2009).

[22] R. Bereczky, G. Kowarik, F. Aumayr, and K. Tökési, Nucl. Instrum. Methods Phys. Res., Sect. B **267**, 317 (2009).

[23] G. Kowarik, R. J. Bereczky, F. Aumayr, and K. Tökési, Nucl. Instrum. Methods Phys. Res., Sect. B **267**, 2277 (2009).

[24] B. Dassanayake, R. J. Bereczky, S. Das, A. Ayyad, K. Tökési, and J. A. Tanis, Phys. Rev. A **83**, 012707 (2011).

[25] E. Gruber, G. Kowarik, F. Ladening, J. P. Waclawek, F. Aumayr, R. J. Bereczky, K. Tökési, P. Gunacker, T. Schweigler, C. Lemell *et al.*, Phys. Rev. A **86**, 062901 (2012).

[26] G. P. Pokhil, K. A. Vokhmyanina, L. A. Zhilyakov, T. Ikeda, Y. Kanai, Y. Iwai, T. M. Kojima, and Y. Yamazaki, Bull. Russ. Acad. Sci.: Phys. **72**, 638 (2008).

[27] G. P. Pokhil, K. A. Vokhmyanina, and A. I. Mironchik, J. Surf. Invest.: X-Ray, Synchrotron Neutron Tech. **3**, 326 (2009).

[28] G. P. Pokhil, K. A. Vokhmyanina, L. A. Zhilyakov, and T. I. Y. Yamazaki, Bull. Russ. Acad. Sci.: Phys. **74**, 221 (2010).

[29] K. Schiessl, W. Palfinger, C. Lemell, and J. Burgdörfer, Nucl. Instrum. Methods Phys. Res., Sect. B **232**, 228 (2005).

[30] K. Schiessl, W. Palfinger, K. Tökési, H. Nowotny, C. Lemell, and J. Burgdörfer, Phys. Rev. A **72**, 062902 (2005).

[31] K. Schiessl, W. Palfinger, K. Tökési, H. Nowotny, C. Lemell, and J. Burgdörfer, Nucl. Instrum. Methods Phys. Res., Sect. B **258**, 150 (2007).

[32] K. Schiessl, C. Lemell, K. Tökési, and J. Burgdörfer, J. Phys: Conf. Ser. **163**, 012081 (2009).

[33] K. Schiessl, K. Tökési, B. Solleder, C. Lemell, and J. Burgdörfer, Phys. Rev. Lett. **102**, 163201 (2009).

[34] P. Skog, H. Zhang, and R. Schuch, Phys. Rev. Lett. **101**, 223202 (2008).

[35] Y. Kanai, M. Hoshino, T. Kambara, T. Ikeda, R. Hellhammer, N. Stolterfoht, and Y. Yamazaki, Phys. Rev. A **79**, 012711 (2009).

[36] N. Stolterfoht, R. Hellhammer, D. Fink, B. Sulik, Z. Juhász, E. Bodewits, H. M. Dang, and R. Hoekstra, Phys. Rev. A **79**, 022901 (2009).

[37] H. Zhang, P. Skog, and R. Schuch, Phys. Rev. A **82**, 052901 (2010).

[38] N. Stolterfoht, E. Bodewits, R. Hellhammer, Z. Juhász, B. Sulik, V. Bayer, C. Trautmann, and R. Hoekstra, J. Phys: Conf. Ser. **388**, 012049 (2012).

[39] N. Stolterfoht, Nucl. Instrum. Methods Phys. Res., Sect. B (to be published).

[40] R. Hellhammer, P. Sobocinski, Z. D. Pešić, D. Fink, J. Bundesmann, B. Sulik, and N. Stolterfoht, Nucl. Instrum. Methods Phys. Res., Sect. B **233**, 213 (2005).

[41] N. Stolterfoht, R. Hellhammer, B. Sulik, Z. Juhász, V. Bayer, C. Trautmann, E. Bodewits, and R. Hoekstra, Phys. Rev. A **83**, 062901 (2011).

[42] Data sheets for PET (Mylar) from DuPont Teijin Films™, www.dupontteijinfilms.com.

[43] Data sheets for PC (Lexan) from Sabic Innovative Plastics™, www.sabic-ip.com.

[44] J. Frenkel, Phys. Rev. **54**, 647 (1938).

[45] D. K. Davies, J. Phys. D: Appl. Phys. **5**, 162 (1972).

[46] W. D. Gill, J. Appl. Phys. **43**, 5033 (1972).

[47] K. Hayashi, K. Yoshino, and Y. Inuishi, Jpn. J. Appl. Phys. **14**, 39 (1975).

[48] N. Stolterfoht, R. Hellhammer, J. Bundesmann, and D. Fink, Phys. Rev. A **77**, 032905 (2008).

[49] MATHEMATICA, www.wolfram.com.